ORIGINAL PAPER

Effect of demineralization and ball milling treatments on the properties of *Arundo donax* and olive stone-derived biochar

M. Zouari[1,2] · L. Marrot[1,3,4] · D. B. DeVallance[1,2,5]

Abstract

The structural and physio-chemical properties of biochar are crucial to determining biochar's quality and the adequate application. Specifically, the large porosity of biochar has been known as a favorable feature, especially for environmental remediation. In this regard, physical and chemical modifications have been used to improve biochar's porosity which requires high-energy consumption and involves chemical agents. The objective of this study was to prepare biochar with developed porosity using mild treatments. *Arundo donax* and olive stone were demineralized by a water-washing method. Treated and non-treated biomasses were pyrolyzed, and part of the derived samples was subjected to wet ball milling. Samples were characterized with proximate, Fourier transform infrared, particle size, and physisorption analyses. The effect of demineralization depended on the biomass type, as ash reduction only influenced *Arundo donax*-derived biochar, which was attributed to the difference in initial ash content that was relatively low for olive stone. The carbonization yield decreased by 46% for the *Arundo donax* biomass after demineralization. Moreover, demineralization expanded the surface area and total pore volume of the *Arundo donax* biochar. The ball milling was effective in producing micro-sized biochar particles with a mean size ranging between 30 ± 2 μm and 42 ± 2 μm and between 13 ± 1 μm and 22 ± 2 μm for *Arundo donax* and olive stone without and with demineralization, respectively. Ball milling increased the surface area of non-demineralized *Arundo donax* by 47% and demineralized *Arundo donax* by 124%. Additionally, ball milling increased the surface area of non-demineralized olive stone by 65% and demineralized olive stone by 62%.

Graphical abstract
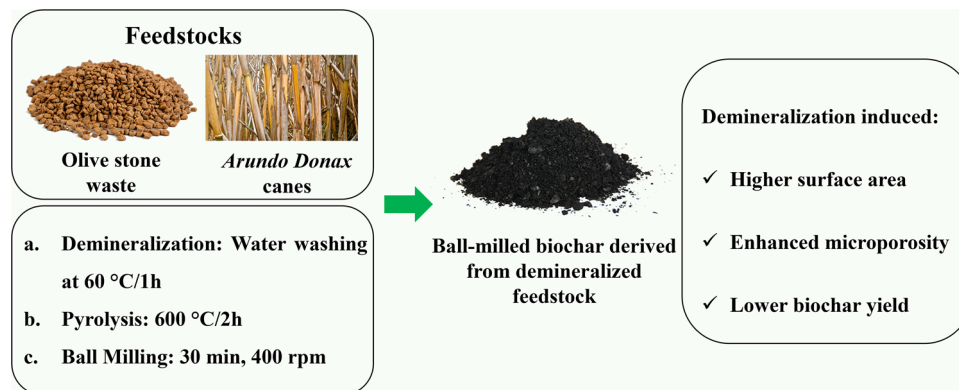
Editorial responsibility: Lifeng Yin.

✉ M. Zouari
   mariem.zouari@innorenew.eu

Extended author information available on the last page of the article

🖉 Springer

Introduction

Arundo donax (AD), also known as *Giant reed*, is an invasive herbaceous species that originated in India but is widespread worldwide. AD is characterized by a fast growth rate and high biomass yield of about 38 tons of dry matter/ha/year (Angelini et al. 2009). In Europe, AD frequently occurs, especially in the southern parts of the Mediterranean area, mainly by rivers, ponds, and lakes. For this reason, AD was ranked 10th among the 100 worst invasive species in the world according to the Global Invasive Species Database (Lowe et al. 2013). The environmental impacts of AD growth can lead to hydrologic alteration and displacement of native species (Lowe et al. 2013). Several attempts have been made to valorize AD. For instance, Flores et al. (2011) manufactured AD-based particleboards for building applications. Results showed that the boards made with AD particles demonstrated mechanical properties comparable to those of the standard industrial wood boards. Raw AD powder was also studied as reinforcement for polymeric composites. Fiore et al. (2014) reported that the addition of 20 wt% of AD fibers (500 μm) in a polylactic acid matrix increased tensile and flexural moduli of the composites by 39% and 45%, respectively, compared to neat polylactic acid. In addition, AD has been utilized as a potential source for energy production via hydrothermal conversion (Krička et al. 2017; Lemons e Silva et al. 2015).

Another abundant feedstock is olive stone (OS), a by-product of olive mills. After oil extraction, vast quantities of waste are left, including olive stones, peels, and pulp. In Europe, olive solid wastes are estimated at 10 million tons annually (European Commission 2022). Notably, the stone part, which represents about 10% of the weight of the olive fruit, contains promising fixed and elemental carbon contents of 16% and 47%, respectively (González et al. 2004), that are needed for biochar (BC) production. Prior studies (Alslaibi et al. 2013; Spahis et al. 2008) prepared OS-derived BC and aimed to increase the surface area using chemical (KOH and $ZnCl_2$) and physical (microwave) activation techniques to improve the potential for wastewater remediation. However, the utilized activation methods have a negative environmental impact due to the application of chemicals and energy consumption. Therefore, it is important to explore greener techniques for developing the porous structure of BC and increasing the range of applications. One possible alternative is the demineralization of biomass.

Valorization of agricultural biomass by thermochemical conversion represents a sustainable approach toward a better environment and a more prosperous economy (Daramola and Ayeni, 2020). The thermal conversion process leads to the generation of bio-oil, gases, and BC. BC is the solid residue derived from the decomposition of organic matter under high temperatures and inert conditions (Lehmann and Stephen 2009). Biomass used to produce BC is abundant, given that it can be prepared from almost any type of organic feedstock, including wastes and industrial by-products. Depending on the temperature, heating rate, and residence time, the thermal conversion process can be categorized into four types: (i) fast pyrolysis which involves the utilization of a heating rate from 10 to 200 °C/s and the dominant products fraction consists of liquid bio-oil (Basu 2013), (ii) slow pyrolysis which applies a heating rate from 0.1 to 0.8 °C/s and mainly generates solid BC along with gas fraction (Basu 2013), (iii) gasification which is usually conducted at extreme temperature (up to 1000 °C) under controlled oxygen conditions and mainly generates gas fraction (Basu 2010), and (vi) hydrothermal conversion which is used for biomass with high moisture content (above 15%) and the solid residue product is often referred as hydrochar. Given its multifunctional properties, BC has been utilized in several applications. For instance, BC was used as an additive in composite materials where it showed potential in enhancing the mechanical and water-resistant properties of polymeric composites (DeVallance et al. 2016; Zouari et al. 2022). BC was also efficiently utilized with polyvinyl alcohol to prepare piezoresistive pressure sensors due to its electrically conductive performance (Nan 2016). Recent research (Marrot et al. 2023) investigated the performance of tung oil/BC-based coating for the protection of wooden facades and reported that BC enhanced the hydrophobicity and the UV irradiation resistance of the tested surfaces. One of the possible primary applications of BC is adsorption. For this reason, BC has been successfully applied in soil (Tomczyk et al. 2019), wastewater (Dwivedi and Dey 2022), and air remediation (Xiang et al. 2022).

The attractiveness of BC lies in the large surface area and high pores volume. These two properties depend on the original biomass type and the pyrolysis parameters (i.e., temperature and time) (Leng et al. 2021). AD and OS wastes represent promising cost-efficient and renewable feedstock for BC production. The characteristics of plant material, such as vascular structure, are likely to contribute to the formation of macropores in the BC, unlike micropores that are mainly generated during the pyrolysis process (Lehmann and Stephen 2009). Another essential biomass feature is the ash content that directly influences pyrolysis because inorganics (i.e., ash minerals) are involved in

volatile cracking and biomass decomposition during thermal conversion (Agblevor and Besler 1996). Raveendran et al. (1995) reported that the occurrence of inorganics negatively impacts the pyrolysis process and BC's surface area. Indeed, during the activation of the BC, minerals can hinder porosity development by blocking the access of activating agents to the internal char structure. Moreover, ash components can limit the potential of BC as an adsorbent by settling around and inside the pores, which reduces the surface area (Jia et al. 2020) and makes pores less available for the adsorbate. AD, for instance, is distinguished by a high ash content (up to $3.56 \pm 0.21\%$ (Krička et al. 2017)) compared to other woody biomasses such as willow ($0.56 \pm 0.08\%$), black locust ($0.77 \pm 0.05\%$), and poplar ($0.59 \pm 0.04\%$) (Klašnja et al. 2013). The high ash content of AD feedstock can limit the application of AD-derived BC for adsorption purposes.

Biomass pre-pyrolysis treatment to remove minerals could enhance BC's porosity and surface area (Paola Giudicianni et al. 2014) and eventually promote BC's adsorption. One method to reduce ash is water washing to eliminate hydrosoluble ash elements such as K, Na, Ca, Cl, S, and Mg. Water washing is a cost-effective, simple, and environmentally friendly technique, as no chemicals are utilized in the process (Paola Giudicianni et al. 2014). Other methods (e.g., acid washing) are less desirable as they have a high environmental impact and lead to the degradation of a portion of the biomass's celluloses and hemicelluloses (Das et al. 2004). Several studies (Chin et al. 2020; Sun et al. 2013) have investigated the demineralization of pyrolyzed biomass (i.e., BC). These studies have reported that ash removal has a favorable effect on enhancing the porous structure of BC. However, research evaluating the impact of raw biomass demineralization (i.e., before carbonization) on the derived BC quality and properties is limited, especially concerning post-treatment ball milling. A few studies (Chandler and Resende 2018; Paola Giudicianni et al. 2014) investigated the influence of raw AD demineralization on the ratio of different pyrolysis products (i.e., gas, solid BC, and bio-oil) and yield. However, they did not provide an in-depth evaluation of the physio-chemical features and porosity of the derived BC.

This study investigated the effect of raw AD and OS demineralization on the derived BC's structural and physio-chemical properties. Moreover, wet ball milling was utilized to further enhance BC porosity development. Results were compared from proximate analysis, FTIR, and physisorption tests of BC from treated and non-treated biomasses.

Materials and methods

Materials and reagents

OS was obtained from Oljarna Krozera Franka Marzi sp. olive oil extraction company (Srgaši, Slovenia) in the form of dry particles (5 mm in size). AD stems were collected from the local area (Kampel, Slovenia). Feedstocks were washed with distilled water and dried at 105 °C for 24 h before processing. AD and OS were separately ground with a cutting mill (Pulverisette 25/19, Fritsch, Idar-Oberstein, Germany) using a 1-mm mesh. Technical nitrogen gas (purity grade 4.8) was utilized for carbonization and thermogravimetric analysis. High-grade nitrogen and carbon dioxide gases with a purity grade of 5.0 were used for physisorption tests.

Biomass demineralization

AD and OS were subjected to hot water stirring wash treatment to reduce the ash content using a method adopted from the literature (Chandler and Resende 2018). The referenced study performed water demineralization of AD at variable temperatures (20, 40, and 60 °C) and concluded that optimal minerals removal was achieved by 1-h washing at 60 °C. Samples of 300 g were first mixed with distilled water (10 g of water per 1 g of dry material). Then, the mixtures were left under continuous stirring for 1 h at 60 °C. At the end of the treatment, the samples were washed under continuous distilled water flow to eliminate the loosened minerals until neutral pH was achieved. The drained samples were then oven-dried for 24 h at 105 °C.

Preparation of biochar: slow pyrolysis and ball milling

For each type of biomass, demineralized and non-demineralized biomass were weighed and placed in thermo-resistant crucibles. The crucibles were then placed in a tube furnace (Nabertherm RSRC 120–1000/13, Nabertherm, Lilienthal, *Germany*) and pyrolyzed under a nitrogen flow rate of 300 L/h and a heating rate of 1500 °C/h to fit in the configuration of slow pyrolysis and to be able to control the thermal inertia of the furnace. The samples were carbonized for 2 h at 600 °C. Indeed, the previous work (Marrot et al. 2021) highlighted an interesting biochar (BC) surface area for hemp stems carbonized at this temperature, combined with an acceptable pyrolysis yield. The obtained BC samples

Table 1 Description of the prepared *Arundo donax* and olive stone biochar samples

Biomass	Sample ID[1]	Treatment
Arundo donax	AD-BC	No treatment
	DAD-BC	Demineralized
	BM-AD-BC	Ball-milled
	BM-DAD-BC	Demineralized and ball-milled
Olive stone	OS-BC	No treatment
	DOS-BC	Demineralized
	BM-OS-BC	Ball-milled
	BM-DOS-BC	Demineralized and ball-milled

AD: *Arundo donax*, OS: Olive stone, BC: Biochar, D: Demineralized, and BM: Ball-milled

were weighed to determine the carbonization yield using Eq. (1).

$$\text{Carbonization yield} = \frac{mi - mf}{mi} \times 100 \tag{1}$$

where *mi* and *mf* are the masses of the raw biomass and the derived BC, respectively.

Part of the obtained samples was further treated by wet ball milling using a planetary ball mill (Pulverisette 5, Fritsch, Idar-Oberstein, Germany). Milling was performed in stainless steel jars (500 mL) in the presence of stainless steel balls (20 mm in diameter), and the balls-to-BC weight ratio was equal to 100. Distilled water was added until the manufacturer's recommended maximum capacity was reached. The BC was milled at a speed of 400 rpm for 30 min. During milling, 30 cycles with a 1-min ON and 5-min OFF procedure were used to avoid temperature increase during milling. The operation conditions were selected based on preliminary optimization. After milling, all the materials were placed in the oven at 105 °C to allow water evaporation and collect BC powder.

In total, eight BC samples were obtained and are described in Table 1.

Characterization of the raw biomasses and the derived biochar

Thermogravimetric analysis (GA 5500, TA Waters Instruments, New Castle, DE, USA) was carried out using 5-mg samples of non-demineralized and demineralized raw biomass. Samples were placed in platinum pans, and the thermal degradation behaviors were observed over a temperature range from 25 to 600 °C and a heating rate of 10 °C/min under a nitrogen atmosphere with a flow rate equal to 25 mL/

min. Three repetitions were performed for each sample, and the average values for degradation temperature points were reported.

Proximate analysis was performed using a thermogravimetric analyzer (TGA801, LECO, Saint-Joseph, MI, USA). The moisture, volatiles, ash, and fixed carbon contents of all samples were determined according to the "ASTM-D7582 in coal" method. Three repetitions were performed for each sample, and the average values were reported.

Surface functional groups were analyzed by Fourier transform infrared (FTIR) spectroscopy using an ALPHA FT-IR Spectrometer (Bruker, Billerica, MA, USA) equipped with ATR (attenuated total reflection) module. The spectra were recorded over a wavelength range from 400 to 4000 cm^{-1} at 4 cm^{-1} resolution. For accurate results, 64 scans were performed, and ten repetitions were done for each sample. The average spectra were then collected and processed using OPUS software.

The particle size analysis was only performed for the ball-milled BC samples. The particle size distribution was measured by laser diffraction using a Horiba Scientific LA-960A2 analyzer (Horiba, Kyoto, Japan), and the refractive index was set to 1.92. For homogeneous particles' dispersion, 1 min of ultrasonication was done before each measurement. Ten repetitions were performed on each sample, and the average values were reported.

Physisorption analysis (Anton Paar Quantachrome Instruments, Boynton Beach, FL, USA) was performed on BC materials using nitrogen and CO_2 gases to evaluate their surface area (SA) and pores distribution according to the Brunauer–Emmett–Teller equation (BET) model and density functional theory (DFT), respectively. Before analysis, samples were degassed under a vacuum for 12 h at 250 °C to remove potential air molecules trapped in the BC's cavities. For BET under nitrogen measurements, the adsorption–desorption isotherms at −196 °C were used to determine the specific SA, total pore volume (TPV), and mesopores (2–50 nm in width) volume. For CO_2 measurements, adsorption–desorption isotherms were collected at 0 °C to determine microporous SA and micropore (<2 nm in width) volume. The collected data were analyzed for statistically significant differences ($\alpha = 5\%$) using a paired *t*-test in

Table 2 Proximate composition of raw non-demineralized and demineralized biomass

Parameters	AD	DAD	OS	DOS
Moisture, %	1.9 ± 0.0	1.6 ± 0.1	1.9 ± 0.0	0.6 ± 0.0
Volatiles, %	75.0 ± 0.2	81.0 ± 0.5	76.0 ± 0.9	77.1 ± 0.1
Ash, %	3.3 ± 0.1	1.1 ± 0.6	0.4 ± 0.1	0.3 ± 0.0
Fixed carbon, %	19.5 ± 0.1	16.2 ± 0.6	22.0 ± 0.9	22.0 ± 0.2

Excel software to evaluate the effect of demineralization and ball milling treatments on BC's porosity.

Results and discussion

Effect of the demineralization on raw *Arundo donax* and olive stone biomass

Physio-chemical properties

Results from proximate analysis of raw AD and OS with and without demineralization are represented in Table 2.

For AD, the results of ash content (3.3 ± 0.1 and $1.1 \pm 0.6\%$) are similar to those reported by Chandler and Resende (2018), that found ash contents of 3.90 and 1.74% before and after demineralization at 60 °C for 1 h, respectively. However, another study (Yang et al. 2020) reported higher ash content in non-washed AD, equal to 6.77%. Even within one plant species, the difference in ash content can be attributed to climate and soil conditions where the plant grew and the sample preparation position within a single plant (Han et al. 2012). The values found for volatiles and fixed carbon in non-demineralized AD (75.0 and 19.5%, respectively) were comparable with the values reported by Yang et al. (2020): 74.59 and 15.36%, respectively.

For OS, the initial ash content ($0.4 \pm 0.1\%$) was similar to findings from Bartocci et al. (2015), who reported 0.49%. However, it was lower than another previous study (Karakaş et al. 2017), which reported 3.34%. This variation in findings for ash content can be due to the differences in the testing method or the olive varieties. In this context, Tanilgan et al. (2007) characterized the physical and chemical properties of five different olives (*Olea europaea L.*) varieties and their oils in Turkey (Gemlik, Kilis, Uslu, Tirilye, and Ayvalik). They found that the inorganics contents of the tested samples differed, and values ranged between 0.6 and 1.2%. Moreover, volatile and fixed carbon percentages of non-washed OS (76.0 and 22.0%, respectively) were divergent compared to the previous finding by Bartocci et al. (2015) and by Karakas et al. (2017b) that reported volatiles and fixed carbon of 87.06% and 12.45%, and 46.42% and 50.24%, respectively.

The demineralization treatment lowered raw AD and OS ash by 48% and 40%, respectively. For AD, the ash content decrease was correlated with an increase in volatiles and a decrease in fixed carbon contents. The presence of high ash percentage in non-demineralized AD likely favored the release of volatiles and the formation of carbon. For OS, however, the volatile and fixed carbon content did not
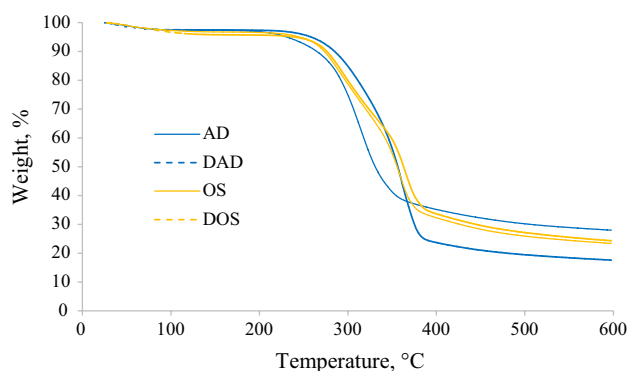

Fig. 1 TGA thermograms of raw non-demineralized and demineralized biomass

Table 3 Thermal degradation points of raw non-demineralized and demineralized biomass

Sample	$T_{10\%}$, °C	T_{max}, °C	Residue at 600 °C, %
AD	265 ± 2	335 ± 1	28 ± 0
DAD	285 ± 3	363 ± 3	19 ± 2
OS	273 ± 1	367 ± 1	26 ± 3
DOS	276 ± 2	377 ± 2	25 ± 1

significantly change due to the demineralization treatment as the material had a naturally low ash content (0.4 ± 0.1).

Thermal degradation properties

Thermogravimetric analysis (TGA) curves for raw non-demineralized and demineralized biomasses are presented in Fig. 1. Values corresponding to 10% of weight loss ($T_{10\%}$), maximum degradation rate (T_{max}), and percentage of final residue at 600 °C are summarized in Table 3.

The decomposition thermograms of all samples (Fig. 1) can be divided into three phases according to the degradation behaviors of the materials. The first phase (25 °C to approximately 200 °C) was characterized by water evaporation and decomposition of light organic compounds and part of hemicelluloses (Yang et al. 2007). The second phase (200–400 °C) was characterized by high mass loss due to the degradation of remaining hemicelluloses and cellulose (Yang et al. 2007). During this phase, lignin starts to decompose as well. The third phase (400–600 °C) was characterized by slow weight loss related to the degradation of lignin

that can decompose gradually from ambient temperature to 900 °C (Yang et al. 2007).

The difference between thermograms of AD with and without demineralization is shown in Fig. 1. $T_{10\%}$ and T_{max} increased by 20 and 28 °C, respectively, after demineralization. This increase reflected the enhancement in the thermal resistance of the demineralized material. The lower thermal stability of non-demineralized AD can be attributed to the combination of two factors.

On the one hand, the increment in thermal stability might be related to the lower hemicellulose content in the treated AD (DAD). Part of the hemicelluloses was likely leached with the minerals during the water-washing process, given their hydro-solubility. Hemicelluloses start degradation at a lower temperature (ranging between 220 and 315 °C) compared to celluloses and lignin that decompose at a higher temperature range (from 315 to 400 °C and from ambient temperature to 900 °C, respectively) (Yang et al. 2007). Therefore, hemicelluloses at lower rates in DAD shifted the thermal decomposition to a higher point. On the other hand, the catalytic effect of ash minerals might have enabled the degradation to start at a lower temperature in the AD sample compared to the demineralized sample. Moreover, the residual char at 600 °C decreased by about 32% after demineralization, which indicates that high ash minerals occurrence in AD contributed to enhancing char formation by activating and catalyzing the thermal conversion of biomass components. Similar results were found by Zhang et al. (2016) when TGA was used to investigate the effect of water washing on the thermal decomposition behaviors of rice husk over a temperature range from 25 to 700 °C (with a heating rate of 20 °C/min). Their findings showed that water washing (at 60 °C for 6 h) increased T_i (initial degradation temperature corresponding to the first increase in degradation rate) and T_{max} by about 30 and 20 °C, respectively, and decreased the final char residue that went from 32.60 to 27.94% for non-washed and washed rice husk, respectively. The enhancement in thermal stability and decrement in final char percentage was assigned to the removal of alkali metals (i.e., ash) involved in catalyzing thermal conversion reactions and promoting char formation. Grafmüller et al. (2022) studied the effect of ash addition on the thermal stability of the derived BC during the pyrolysis of softwood biomass. They reported that the increase of 0–42.6 wt% ash content correlated with a decrease in the material's thermal resistance. They observed that the exothermic peaks in the degradation thermograms obtained from diffraction scanning calorimetry analysis shifted and that the maximum degradation

Table 4 Carbonization yields results

Original biomass	AD	DAD	OS	DOS
Yield in BC, %	23.5	12.7	24.6	23.9

temperature decreased by 43 °C, 51 °C, and 55 °C with the addition of 7.3%, 8.9%, and 42.6% of ash, respectively. They explained that the acceleration in thermal decomposition is assigned to the catalytic effect of ash components.

For OS biomass, the degradation temperature points ($T_{10\%}$ and T_{max}) and final residue percentages were similar for non-demineralized and demineralized materials (Table 3). This similarity suggests that the demineralization treatment did not significantly affect the degradation process of OS. These findings are likely related to OS's initially low ash content ($0.4 \pm 0.1\%$). Moreover, the OS appeared to be more resistant to thermal decomposition ($T_{10\%} = 273 \pm 1$ °C) compared to AD ($T_{10\%} = 265 \pm 2$ °C), which might be related to the original chemical composition of the two biomasses. Specifically, OS has been reported to have a lower hemicellulose content of 21.9% (Heredia-Moreno et al. 1987) compared to the 34.02% hemicellulose content of AD (Suárez et al. 2021). This lower hemicellulose content would result in higher thermal resistance of OS compared to AD. The lower demineralization yield of AD (83%) compared to OS (86%) is likely due to the partial loss of soluble hemicelluloses during washing. However, further investigation of the chemical composition of AD and OS must be performed to confirm this assumption.

Carbonization yield

The BC yield percentages are summarized in Table 4.

In the case of AD, the demineralization caused a 46% decrease in the BC yield, likely due to the reduction in ash components that have the primary role in the volatile exhaust and BC formation. It is noteworthy that these findings correlate with the TGA results, where a decrease in the final char residue from AD after demineralization was observed (Table 3). Ash components are responsible for favoring the cracking of volatiles released from natural polymer degradation into permanent gases, promoting BC formation and increasing yield.

Prior research (Chandler and Resende 2018) reported that BC yield from ground AD (with average particle size equal to 373 μm) by water washing at 60 °C for 1 h and pyrolyzing

at 475 °C was equal to 17.5% and 13.2%, respectively, before and after demineralization. These values are much smaller than those found in the current study (31.85% and 12.67%), even though a higher carbonization temperature (600 °C) was utilized. However, Yang et al. (2020) reported that AD yielded 33.22% of BC after pyrolysis at 600 °C, which is comparable to the findings reported in this study. The differences between BC yields can be related to the difference in the original AD composition (i.e., the ratio of hemicelluloses, cellulose, and lignin) that can vary with the species, age of the plant, and the period of the year when it was harvested. Additionally, biomass particle size before carbonization and the utilized heating rate are likely to influence the final yield (Angın, 2013; Demirbas 2004).

Paola et al. (2014) studied the physio-chemical properties of demineralization AD and the derived BC. They reported that ash content decrease was correlated with a reduction in BC yield that was attributed to the enhanced devolatilization (i.e., fewer amounts of volatiles were released during pyrolysis) upon minerals reduction. In addition, they stated that the pyrolysis of water-washed AD samples produced lower yields of gases such as H_2, CO, and CO_2 compared to the non-treated sample due to the removal of alkali ions. They concluded that the decrease in H_2 yield in the water-washed sample suggests that alkali metals have a catalytic role in BC gasification reactions (Paola Giudicianni et al. 2014). Grafmüller et al. (2022) observed that the carbonization yield increased linearly with increasing the ash percentage from 0 to 8.9 wt%. However, a further increase in ash rate (up to 42.6 wt%) did not cause any significant change in the yield. They justified that the occurrence of alkali elements in the ash helped the BC formation by catalyzing primary and secondary pyrolysis reaction pathways.

For non-demineralized OS, the obtained yield (24.6%) is lower compared to findings from the previous research (Karakaş et al. 2017), where a 31.44% yield was reported for OS carbonized at the same temperature (600 °C). The demineralization did not significantly affect the carbonization yield, as the BC amount obtained from OS and DOS was similar (24.6% and 23.9%, respectively). These findings can be justified by the relatively low initial minerals content in raw OS (0.44%) confirmed by proximate analysis (Table 2).

Thus, the demineralization treatment did not influence the BC yield.

Effect of demineralization on *Arundo donax* and olive stone-derived biochar

Physio-chemical properties

Table 5 represents the results for moisture, volatiles, ash, and fixed carbon contents of BC derived from non-demineralized and demineralized AD and OS feedstocks.

For non-demineralized AD-derived BC, results for volatiles, ash, and fixed carbon contents ($16.6 \pm 1.0\%$, $11.0 \pm 0.1\%$, and $65.6 \pm 1.0\%$, respectively) were comparable with findings from Zhao et al. (2017) who reported $14.72 \pm 0.41\%$, $6.85 \pm 0.16\%$, and $75.20 \pm 0.47\%$, respectively, for AD-BC prepared at 500 °C for 2 h, and $7.48 \pm 0.81\%$, $6.20 \pm 0.11\%$, and $81.30 \pm 0.86\%$, respectively, for AD-BC prepared at 800 °C for 2 h. Volatiles and ash percentages were lower in BC derived from the demineralized AD (DAD-BC) by 20.7 and 69.2% compared to BC derived from the non-demineralized precursor (AD-BC). As explained in Sect. "Carbonization yield," inorganics (i.e., ash) facilitate the volatilization of gases during cellulose, hemicellulose, and lignin thermal degradation. Therefore, after the reduction of ash content, the volatile rate also was reduced. However, demineralization increased the fixed carbon content from $65.6 \pm 1.0\%$ to $78.3 \pm 0.8\%$, which can be attributed to the higher organic content of the treated biomass compared to the same amount of non-treated sample.

For OS-BC, volatiles ($13.0 \pm 0.6\%$) and fixed carbon ($83.1 \pm 0.5\%$) content results agreed with prior research (Bartocci et al. 2015) for OS carbonized at 600 °C that reported 11.45% volatile and 76.75% fixed carbon contents. Nevertheless, the same study reported a much higher ash content of about 11.80% compared to results found in this study ($0.9 \pm 0.2\%$). Demineralization of OS reduced the ash content in the derived BC by 38.3%, while no obvious changes were observed in volatiles and fixed carbon rates. It is also worth mentioning that the fixed carbon content in OS-BC was higher than AD-BC, which is likely related to the differences in the chemical composition of the two feedstocks.

Fourier Transfer Infrared spectroscopy

Fourier transform infrared (FTIR) spectra of raw and carbonized specimens are represented in Fig. 2.

Table 5 Proximate composition of *Arundo donax* and olive stone-derived biochar

Parameters	AD-BC	DAD-BC	OS-BC	DOS-BC
Moisture, %	6.7 ± 0.1	5.1 ± 0.8	3.0 ± 0.0	2.8 ± 0.1
Volatiles, %	16.6 ± 1.0	13.2 ± 0.3	13.0 ± 0.6	13.5 ± 0.8
Ash, %	11.0 ± 0.1	3.4 ± 0.2	0.9 ± 0.2	0.6 ± 0.0
Fixed carbon, %	65.6 ± 1.0	78.3 ± 0.8	83.1 ± 0.5	83.1 ± 0.8

Fig. 2 FTIR spectra of non-demineralized and demineralized *Arundo donax* **a** and olive stone **b** biomass and the derived biochar
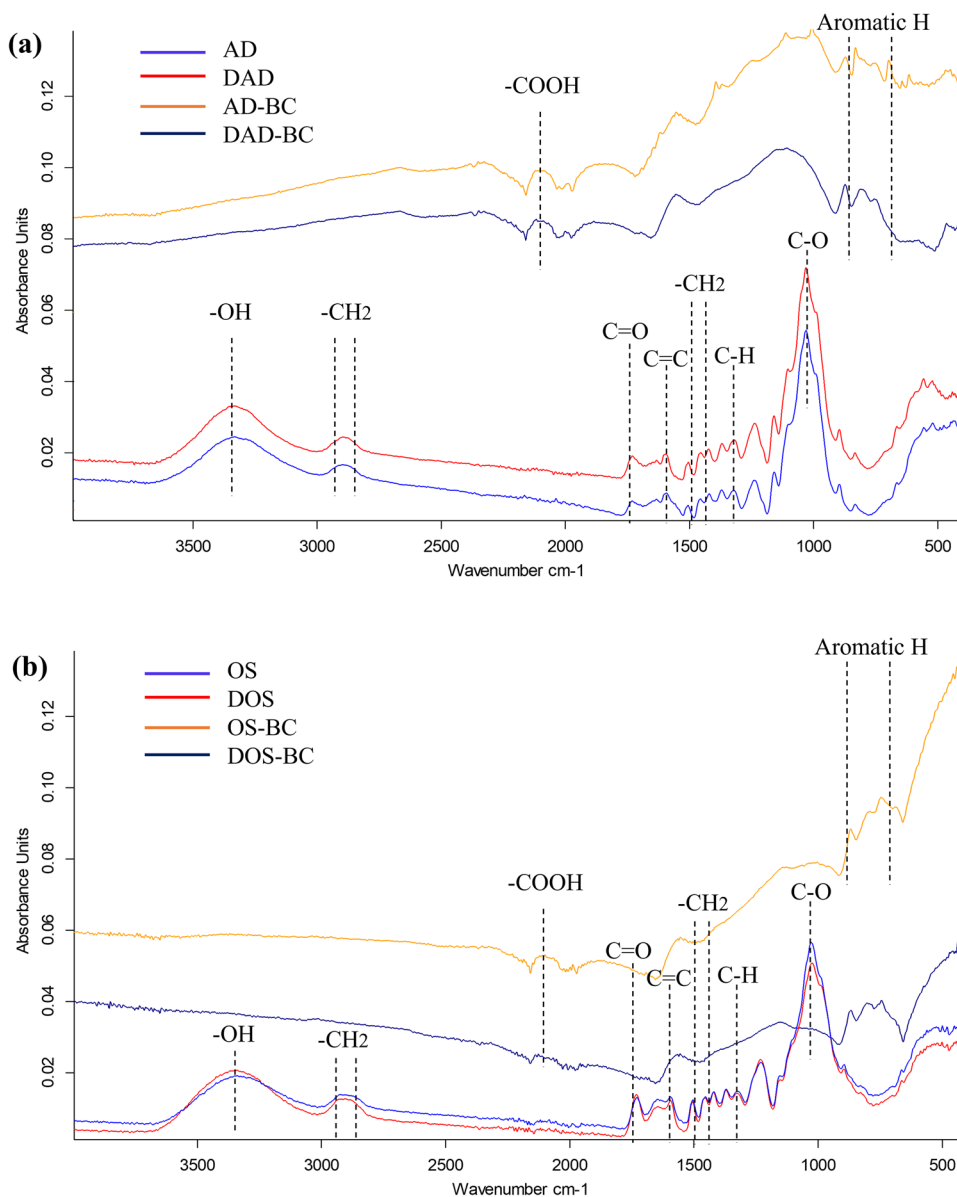
Regardless of the biomass type (AD or OS), non-demineralized and demineralized raw and carbonized materials exhibited similar bands in the FTIR spectra.

The FTIR spectra of the raw AD and OS (non-demineralized and demineralized) exhibited a wide band at 3430 cm^{-1} that corresponds to hydroxyl groups from water molecules. This band was not visible for the corresponding BC samples due to water evaporation during the pyrolysis. Janu et al. (2021) studied surface functional groups of BC derived from different feedstocks and prepared at different temperatures (from 300 to 750 °C). They reported that for Norway spruce wood chip-derived BC samples, H-bonded hydroxyl groups associated with wavenumbers ranging between 3200 and 3700 cm^{-1} tend to be degraded at pyrolysis temperatures from 300 to 600 °C.

Bands at 2850 and 2920 cm^{-1} can be attributed to CH_2 stretching vibrations (Zhao et al. 2017). These bands were only detected in the raw materials with and without demineralization but were absent in the spectra of carbonized materials, probably because of the degradation of a major part of natural polymers (i.e., hemicelluloses, celluloses, and lignin) due to the high pyrolysis temperature (600 °C).

The wide band at 2120 cm^{-1} can be assigned to carboxyl vibrations (Angın, 2013). This band was visible for all BC

specimens from AD and OS; however, it was not detected in raw biomass. This observation can be justified by the increase in carbon content and the volatilization of hydrogen and oxygen during pyrolysis, which is correlated with the proximate analysis results (Table 2 and Table 5) that confirmed the higher fixed carbon contents of all BC samples compared to the corresponding original biomass. In this context, Shafidazeh et al. (1985) stated that during pyrolysis of the biomass at a temperature above 350 °C, the aliphatic carbon units present in cellulose polymers are converted into a mixture of aliphatic, alkene, aromatic, carboxyl, and carbonyl structures. However, the peak at 1750 cm^{-1} corresponding to C=O carbonyl groups was mainly observed in the spectra of the raw materials.

The peak at 1580 cm^{-1} identified in all BC samples can be related to the occurrence of C=C bonds with conjugation of π electrons (Kaczmarczyk 2013) due to high electronegativity functional groups. The same band was detected by Magioglou et al. (2019) in olive stone BC prepared at 850 °C.

Peaks between 1400 and 1500 cm^{-1} correspond to aromatic C and aliphatic CH$_2$– groups present in lignin polymers (Janu et al. 2021). These functions were visible in raw materials but slightly disappeared in the carbonized samples, likely due to the degradation of lignin polymers during pyrolysis.

The band at 1385 cm^{-1}, corresponding to aromatic C–H stretching, was sharper in the raw feedstock and diminished in all BC spectra. These results may have been due to these groups' deterioration at the high carbonization temperature (600 °C). In this context, Zhao et al. (2017) characterized AD-derived BC samples prepared at 500 and 800 °C. They reported that 1385 cm^{-1} vibration could be observed only in FTIR spectra of AD-BC prepared at 500 °C while the vibration disappeared at a higher temperature.

The band at 1050 cm^{-1} can be attributed to the valence fluctuation of C–O bonds in cellulose and hemicellulose. It was visible only in the spectra of raw biomasses due to the degradation of cellulose and hemicellulose during the thermal conversion.

Vibrations between 700 and 900 cm^{-1} are attributed to aromatic hydrogen structures (Angın, 2013; Hossain et al. 2011). These structures were less visible before carbonization, which reflects the aromatic character (i.e., less polar character) of the obtained BC compared to the origin biomass.

Overall, the FTIR analysis showed that the demineralization treatment did not influence the functional group composition in either raw or carbonized AD and OS, as the same spectra were obtained for samples with and without demineralization.

Particle size of ball-milled biochar samples

Size distributions of ball-milled BC samples derived from non-demineralized and demineralized AD and OS are listed in Table 6. Percentile values D_{10}, D_{50}, and D_{90} are statistical

Table 6 Particle size representative diameters of the ball-milled biochar samples

Cumulative particle size distribution	Particle size (μm)			
	BM-AD-BC	BM-DAD-BC	BM-OS-BC	BM-DOS-BC
D_{10}	4 ± 1	5 ± 1	2 ± 1	3 ± 1
D_{50}	16 ± 1	18 ± 2	11 ± 1	11 ± 2
D_{90}	70 ± 3	104 ± 2	25 ± 1	53 ± 2
Mean	30 ± 2	42 ± 2	13 ± 1	22 ± 2

Table 7 Porosity evaluation of biochar samples

Sample	N$_2$	CO$_2$			
	BET SA[1], m^2/g	TPV[2], cc/g	Mesopores volume, cc/g	Microporous SA, m^2/g	Micropores volume, cc/g
AD-BC	45	0.003	0.003	516	0.138
DAD-BC	172	0.091	0.067	601	0.165
OS-BC	266	0.127	0.029	597	0.162
DOS-BC	268	0.115	0.036	595	0.163
BM-AD-BC	66	0.054	0.035	535	0.132
BM-DAD-BC	385	0.170	0.038	563	0.152
BM-OS-BC	438	0.192	0.038	567	0.152
BM-DOS-BC	435	0.194	0.040	565	0.154

[1]SA: Surface area and [2]TPV: Total pore volume

Table 8 Paired *t*-test results

Compared pairs	*P*-values		
	BET surface area	Total pore volume	Microporous surface area
AD-BC/DAD-BC	0.004[*]	0.002[*]	0.008[*]
OS-BC/DOS-BC	0.398	0.080	0.102
AD-BC/BM-AD-BC	0.020[*]	0.007[*]	0.397
DAD-BC/BM-DAD-BC	0.020[*]	0.009[*]	0.392
OS-BC/BM-OS-BC	0.030[*]	0.040[*]	0.005[*]
DOS-BC/BM-DOS-BC	0.020[*]	0.040[*]	0.006[*]

* Statistically significant difference

representatives for the cumulative particle size distribution where they indicate the size below which 10%, 50%, and 90% of all particles are obtained, respectively.

Regardless of the sample type, the particle size distributions were fitted into the micro-size range (Table 6). The obtention of micro-sized particles shows that ball milling treatment enabled the size reduction even when applied for a relatively short duration (30 min). The effectiveness of ball milling in BC's size reduction was previously confirmed by Zhuang et al. (2021), regardless of the biomass type and carbonization conditions.

Overall, AD-derived BC had a slightly higher particle size distribution in both non-demineralized AD (4 ± 1 μm and 70 ± 3 μm) and demineralized AD (5 ± 1 μm and 104 ± 2 μm) compared to non-demineralized OS (2 ± 1 μm and 25 ± 1 μm) and demineralized OS (3 ± 1 μm to 53 ± 2 μm) derived BC. The variation in particle size can be related to the shape of the pristine BC particles before ball milling. AD generated thin sheet-shaped BC particles, while OS generated more solid and round particles which probably facilitated the crushing operation during the ball milling process. A previous study by Naito et al. (1998) emphasized the determinant effect of particle shape on particle size distribution measurements and reported that rod-shaped particles (i.e., less round particles) appear in the wide size range when using the laser diffraction technique.

Regardless of the biomass type, samples from demineralized biomass exhibited larger sizes which were attributed to the extent of dispersion of particles in the aqueous media during size measurement. For AD, the occurrence of ash minerals likely favored the dispersion of BC particles due to the electrostatic forces between minerals and carbon elements in BC. These forces were lower in BC samples prepared from demineralized biomass, which affected the dispersion and allowed the aggregation of carbon particles that appeared big during the analysis. However, for OS, the ash content was slightly different after demineralization.

Therefore, the particle size variation could be just related to the potential non-homogeneous dispersion of the particles during the ultrasonication and analysis.

Porosity of the biochar samples

The surface area (SA) and pores characteristics of the pristine and ball-milled BC samples from N_2 and CO_2 physisorption isotherms are shown in Table 7. Results from the statistical comparison are presented in Table 8. The difference between the compared pairs is considered statistically significant if $P \leq 0.05$.

The SA and total pores volume (TPV) of BC prepared from demineralized AD (DAD-BC) were higher by 3.8- and 30.3-fold, respectively, compared to BC derived from non-demineralized AD (AD-BC). Moreover, the microporous SA and micropores volume of the same sample (DAD-BC) increased by 16% and 25%, respectively. The demineralization of raw AD contributed efficiently to BC's porous structure, manifested by a statistically significant increase in SA, TPV, and microporous SA (Table 8). The occurrence of ash minerals favors the removal of volatiles during pyrolysis and leads to larger pores (i.e., mesopores). When the ash content was reduced in the AD feedstock, lower amounts of volatiles were released, and the porosity of the obtained BC was more composed of narrow micropores (i.e., pore size < 2 nm). Furthermore, the increment in SA and TPV after demineralization can be assigned to removing minerals that were settling and blocking the BC's cavities. Thus, BC derived from the demineralized AD has more free pores and exposed SA. In a similar experiment, Paola et al. (2014) demineralized AD biomass using distilled water, HCl 0.1 M, and HCl 3.5 at 30 °C. They also observed a sharp increase in BET SA regardless of the utilized demineralization solution. For OS-derived BC, minor differences were observed in SA and porosity of BC prepared from treated and non-treated biomass. The statistical comparison between SA, TPV, and

microporous SA of OS-BC and DOS-BC was not statistically different (Table 8).

Regardless of the feedstock type, ball milling positively affected BC's porosity. As compared to the pristine samples (i.e., non-ball-milled samples), the SA of ball-milled BC from non-demineralized and demineralized AD increased by 47% and 124%, respectively. The SA of ball-milled BC from non-demineralized and demineralized OS increased by 65% and 62%, respectively. Similarly, the TPV of the BC increased by 1700%, 87%, 51%, and 69%, respectively. The increment in SA and TPV after ball milling was statistically significant for all samples (Table 8). Nevertheless, the microporous SA and micropores volume decreased slightly after ball milling. The decrease in microporosity was attributed to the widening and fusion of smaller pores (i.e., micropores) under mechanical crushing during ball milling. This process generated larger pores and exposed the internal BC structure. Similarly, Lyu et al. (2018) reported that BET SA of bamboo BC prepared by carbonization at 600 °C for 2 h increased by 368% after ball milling at 300 rpm for 12 h compared to non-ball-milled bamboo BC. They explained that ball milling increased the external and internal SA by reducing the particle size and opening new internal pores. Similarly, Xiang et al. (2020) stated that the BET SA of hickory wood-derived BC prepared at 300 °C, 450 °C, and 600 °C (2 h) increased by 7-, 29-, and 1.4-fold, respectively, after ball milling (at 300 rpm for 12 h) which was assigned to the opening of new pores by mean of milling.

Conclusion

Pre-carbonization biomass demineralization was investigated to identify changes in the physio-chemical properties and porosity of the derived biochar (BC). Moreover, the ability of BC's ball milling to enhance the porosity was evaluated. The main outcomes of the study were:

- The demineralization decreased the carbonization yield by 46% in the case of *Arundo donax* (AD). However, no difference in carbonization yield was observed for olive stone (OS).
- The BC derived from demineralized AD had surface area and total pores volume that were 4 and 30 times higher compared to those of BC derived from non-demineralized AD, respectively. The demineralization process increased the AD-derived BC microporous volume by

25%. However, there was no change in the porosity and microporosity of OS-derived BC.
- The demineralization effect depended on the biomass type, and it was more visible when the biomass had a high initial ash content, such as AD.
- The ball milling treatment enhanced the surface area of the BC regardless of the feedstock type. However, ball milling slightly decreased the microporosity by widening and fusing narrow micropores under mechanical crushing.

Overall, raw biomass demineralization and BC ball milling were determined to be promising green approaches to fabricating porous BC without using chemical agents, in a view of an application as adsorbent, which will be the focus of the next study. Further research is forecasted to determine the ash elements composition before and after the demineralization process and to identify the key elements that were removed by the treatment and comprehensively understand the induced changes in the BC's properties.

Data availability Not applicable.

Declarations

Conflict of interest The authors have no relevant financial or non-financial interests to disclose.

References

Agblevor FA, Besler S (1996) Inorganic compounds in biomass feedstocks. 1. effect on the quality of fast pyrolysis oils. Energy Fuels 10:293–298. https://doi.org/10.1021/ef950202u

Alslaibi TM, Abustan I, Ahmad MA, Foul AA (2013) Cadmium removal from aqueous solution using microwaved olive stone activated carbon. J Environ Chem Eng 1:589–599. https://doi.org/10.1016/j.jece.2013.06.028

Angelini LG, Ceccarini L, Di Nassi o Nasso N, Bonari E (2009) Comparison of *Arundo donax* L and Miscanthus x giganteus in a long-term field experiment in Central Italy: analysis of productive characteristics and energy balance. Biomass Bioenergy 33:635–643. https://doi.org/10.1016/j.biombioe.2008.10.005

Angın D (2013) Effect of pyrolysis temperature and heating rate on biochar obtained from pyrolysis of safflower seed press cake. Bioresour Technol 128:593–597. https://doi.org/10.1016/j.biortech.2012.10.150

Bartocci PD'Amico, M, Moriconi N, Bidini G, Fantozzi F, (2015) Pyrolysis of Olive Stone for Energy Purposes. Energy Procedia, 70th Conference of the Italian Thermal Machines Engineering Association, ATI2015 82: 374–380 https://doi.org/10.1016/j.egypro.2015.11.808

Basu P, (2010). Chapter 5 Gasification Theory and Modeling of Gasifiers, in: Basu, P (Ed), Biomass Gasification and Pyrolysis. Academic Press, Boston, 117-165 https://doi.org/10.1016/B978-0-12-374988-8.00005-2

Basu P, (2013) Chapter 5 - Pyrolysis, in: Basu, P. (Ed.), Biomass Gasification, Pyrolysis and Torrefaction (Second Edition). Academic Press, Boston, 147–176 https://doi.org/10.1016/B978-0-12-396488-5.00005-8

Chandler DS, Resende FLP (2018) Effects of warm water washing on the fast pyrolysis of *Arundo Donax*. Biomass Bioenergy 113:65–74. https://doi.org/10.1016/j.biombioe.2018.03.008

Chin KL, Lee CL, H'ng PSE, Rashid U, Paridah MT, Khoo PS, Maminski M (2020) Refining micropore capacity of activated carbon derived from coconut shell via deashing post-treatment. BioResources 15:7749–7769

European Commission, (2022). LIFE 3.0 - LIFE Project Public Page [WWW Document]. Life Public Database Eur. URL https://webgate.ec.europa.eu/life/publicWebsite/index.cfm?fuseaction=search.dspPage&n_proj_id=2871 (accessed 7.11.22).

Daramola MO, Ayeni AO Eds, (2020). Valorization of Biomass to Value-Added Commodities: current Trends, Challenges, and Future Prospects, Green Energy and Technology. Springer International Publishing, Cham. https://doi.org/10.1007/978-3-030-38032-8

Das D, Gaur V, Verma N (2004) Removal of volatile organic compound by activated carbon fiber. Carbon 42:2949–2962. https://doi.org/10.1016/j.carbon.2004.07.008

Demirbas A (2004) Effects of temperature and particle size on biochar yield from pyrolysis of agricultural residues. J Anal Appl Pyrolysis 72:243–248. https://doi.org/10.1016/j.jaap.2004.07.003

DeVallance DB, Oporto GS, Quigley P (2016) Investigation of hardwood biochar as a replacement for wood flour in wood–polypropylene composites. J Elastomers Plast 48:510–522. https://doi.org/10.1177/0095244315589655

Dwivedi S, Dey S (2022) Review on biochar as an adsorbent material for removal of dyes from waterbodies. Int J Environ Sci Technol. https://doi.org/10.1007/s13762-022-04364-9

Fiore V, Botta L, Scaffaro R, Valenza A, Pirrotta A (2014) PLA based biocomposites reinforced with *Arundo donax* fillers. Compos Sci Technol 105:110–117. https://doi.org/10.1016/j.compscitech.2014.10.005

Flores JA, Pastor JJ, Martinez-Gabarron A, Gimeno-Blanes FJ, Rodríguez-Guisado I, Frutos MJ (2011) *Arundo donax* chipboard based on urea-formaldehyde resin using under 4mm particles size meets the standard criteria for indoor use. Ind Crops Prod 34:1538–1542. https://doi.org/10.1016/j.indcrop.2011.05.011

Giudicianni P, Cardone G, Cavaliere A, Ragucci R (2014) Effect of feedstock demineralization on physico-chemical characteristics of *Arundo donax* derived biochar. Chem Eng Trans 37:85–90. https://doi.org/10.3303/CET1437015

González JF, González-García CM, Ramiro A, González J, Sabio E, Gañán J, Rodríguez MA (2004) Combustion optimisation of biomass residue pellets for domestic heating with a mural boiler. Biomass Bioenerg 27:145–154. https://doi.org/10.1016/j.biombioe.2004.01.004

Grafmüller J, Böhm A, Zhuang Y, Spahr S, Müller P, Otto TN, Bucheli TD, Leifeld J, Giger R, Tobler M, Schmidt H-P, Dahmen N, Hagemann N (2022) Wood ash as an additive in biomass pyrolysis: effects on biochar yield, properties, and agricultural performance. ACS Sustain Chem Eng 10:2720–2729. https://doi.org/10.1021/acssuschemeng.1c07694

Han W, Chen Y, Zhao F-J, Tang L, Jiang R, Zhang F (2012) Floral, climatic and soil pH controls on leaf ash content in China's terrestrial plants. Glob Ecol Biogeogr 21:376–382. https://doi.org/10.1111/j.1466-8238.2011.00677.x

Heredia-Moreno A, Guillén-Bejarano R, Fernández-Bolaños J, Rivas-Moreno M (1987) Olive stones as a source of fermentable sugars. Biomass 14:143–148. https://doi.org/10.1016/0144-4565(87)90016-3

Hossain MK, Strezov V, Chan KY, Ziolkowski A, Nelson PF (2011) Influence of pyrolysis temperature on production and nutrient properties of wastewater sludge biochar. J Environ Manage 92:223–228. https://doi.org/10.1016/j.jenvman.2010.09.008

Janu R, Mrlik V, Ribitsch D, Hofman J, Sedláček P, Bielská L, Soja G (2021) Biochar surface functional groups as affected by biomass feedstock biochar composition and pyrolysis temperature. Carbon Resour Convers 4:36–46. https://doi.org/10.1016/j.crcon.2021.01.003

Jia Y, Hu Z, Mu J, Zhang W, Xie Z, Wang G (2020) Preparation of biochar as a coating material for biochar-coated urea. Sci Total Environ 731:139063. https://doi.org/10.1016/j.scitotenv.2020.139063

Kaczmarczyk B (2013) FTIR study of conjugation in selected aromatic polyazomethines. J Mol Struct 1048:179–184. https://doi.org/10.1016/j.molstruc.2013.05.036

Karakaş C, Özçimen D, İnan B (2017) Potential use of olive stone biochar as a hydroponic growing medium. J Anal Appl Pyrolysis 125:17–23. https://doi.org/10.1016/j.jaap.2017.05.005

Klašnja B, Orlović S, Galić Z (2013) Comparison of different wood species as raw materials for bioenergy South-East Eur. For 4:81–88. https://doi.org/10.15177/seefor.13-08

Krička T, Matin A, Bilandžija N, Jurišić V, Antonović A, Voća N, Grubor M (2017) Biomass valorisation of *Arundo donax* L.,

Miscanthus × giganteus and Sida hermaphrodita for biofuel production. Int Agrophysics 31:575–581. https://doi.org/10.1515/intag-2016-0085

Lehmann J, Stephen J, (2009). Biochar for Environmental Management: science, technology and implementation, 2nd edition. ed. Routledge Taylor & Francis Group.

Lemons e silva CF, Schirmer MA, Maeda RN, Barcelos CA, Pereira N (2015) Potential of giant reed (*Arundo donax* L.) for second generation ethanol production. Electron J Biotechnol 18:10–15. https://doi.org/10.1016/j.ejbt.2014.11.002

Leng L, Xiong Q, Yang L, Li H, Zhou Y, Zhang W, Jiang S, Li H, Huang H (2021) An overview on engineering the surface area and porosity of biochar. Sci Total Environ 763:144204. https://doi.org/10.1016/j.scitotenv.2020.144204

Lowe S, Browne M, Boudjelas S, De Poorter M, (2013). 100 of the World's Worst Invasive Alien Species: a selection from the Global Invasive Species Database.

Lyu H, Gao B, He F, Zimmerman AR, Ding C, Huang H, Tang J (2018) Effects of ball milling on the physicochemical and sorptive properties of biochar: experimental observations and governing mechanisms. Environ Pollut 233:54–63. https://doi.org/10.1016/j.envpol.2017.10.037

Magioglou E, Frontistis Z, Vakros J, Manariotis ID, Mantzavinos D (2019) Activation of persulfate by biochars from valorized olive stones for the degradation of sulfamethoxazole. Catalysts 9:419. https://doi.org/10.3390/catal9050419

Marrot L, Candelier K, Valette J, Lanvin C, Horvat B, Legan L, DeVallance DB (2021) Valorization of hemp stalk waste through thermochemical conversion for energy and electrical applications. Waste Biomass Valorization 13:2267–2285. https://doi.org/10.1007/s12649-021-01640-6

Marrot L, Zouari M, Schwarzkopf M, DeVallance DB (2023) Sustainable biocarbon/tung oil coatings with hydrophobic and UV-shielding properties for outdoor wood substrates. Prog Org Coat 177:107428. https://doi.org/10.1016/j.porgcoat.2023.107428

Naito M, Hayakawa O, Nakahira K, Mori H, Tsubaki J (1998) Effect of particle shape on the particle size distribution measured with commercial equipment. Powder Technol 100:52–60. https://doi.org/10.1016/S0032-5910(98)00052-7

Nan N (2016) Development of polyvinyl alcohol/wood-derived carbon thin films: influence of processing parameters on mechanical, thermal, and electrical properties. Nat Resour Design West Virginia Univ, Morgantown, WV, USA, Davis College of Agriculture

Raveendran K, Ganesh A, Khilar KC (1995) Influence of mineral matter on biomass pyrolysis characteristics. Fuel 74:1812–1822. https://doi.org/10.1016/0016-2361(95)80013-8

Shafizadeh F, (1985) Pyrolytic reactions and products of biomass, in: Overend RP, Milne TA, Mudge LK Eds, fundamentals of thermochemical biomass conversion. Springer Netherlands, Dordrecht, 183-217 https://doi.org/10.1007/978-94-009-4932-4_11

Spahis N, Addoun A, Mahmoudi H, Ghaffour N (2008) Purification of water by activated carbon prepared from olive stones desalination european desalination society and center for research

and technology hellas (CERTH) Sani Resort 22–25 April 2007. Halkidiki Greece 222:519–527. https://doi.org/10.1016/j.desal.2007.02.065

Suárez L, Castellano J, Romero F, Marrero MD, Benítez AN, Ortega Z (2021) Environmental hazards of giant reed (*Arundo donax* L.) in the Macaronesia Region and Its characterisation as a potential source for the production of natural fibre composites. Polymers 13:2101. https://doi.org/10.3390/polym13132101

Sun K, Kang M, Zhang Z, Jin J, Wang Z, Pan Z, Xu D, Wu F, Xing B (2013) Impact of deashing treatment on biochar structural properties and potential sorption mechanisms of phenanthrene. Environ Sci Technol 47:11473–11481. https://doi.org/10.1021/es4026744

Tanilgan K, Özcanb M, Ünver A (2007) Physical and chemical characteristics of five Turkish olive (Olea europea L.) varieties and their oils. Grasas Aceites 58(2):142–147. https://doi.org/10.3989/gya.2007.v58.i2.78

Tomczyk A, Boguta P, Sokołowska Z (2019) Biochar efficiency in copper removal from Haplic soils. Int J Environ Sci Technol 16:4899–4912. https://doi.org/10.1007/s13762-019-02227-4

Xiang W, Zhang X, Chen K, Fang J, He F, Hu X, Tsang DCW, Ok YS, Gao B (2020) Enhanced adsorption performance and governing mechanisms of ball-milled biochar for the removal of volatile organic compounds (VOCs). Chem Eng J 385:123842. https://doi.org/10.1016/j.cej.2019.123842

Xiang W, Zhang X, Cao C, Quan G, Wang M, Zimmerman AR, Gao B (2022) Microwave-assisted pyrolysis derived biochar for volatile organic compounds treatment: characteristics and adsorption performance. Bioresour Technol 355:127274. https://doi.org/10.1016/j.biortech.2022.127274

Yang H, Yan R, Chen H, Lee DH, Zheng C (2007) Characteristics of hemicellulose, cellulose and lignin pyrolysis. Fuel 86:1781–1788. https://doi.org/10.1016/j.fuel.2006.12.013

Yang J, Wang X, Shen B, Hu Z, Xu L, Yang S (2020) Lignin from energy plant (*Arundo donax*): pyrolysis kinetics, mechanism and pathway evaluation. Renew Energy 161:963–971. https://doi.org/10.1016/j.renene.2020.08.024

Zhang S, Dong Q, Zhang L, Xiong Y (2016) Effects of water washing and torrefaction on the pyrolysis behavior and kinetics of rice husk through TGA and Py-GC/MS. Bioresour Technol Pretreatment of Biomass 199:352–361. https://doi.org/10.1016/j.biortech.2015.08.110

Zhao Y, Huang L, Chen Y (2017) Biochars derived from giant reed (*Arundo donax* L.) with different treatment: characterization and ammonium adsorption potential. Environ Sci Pollut Res 24:25889–25898. https://doi.org/10.1007/s11356-017-0110-3

Zhuang Z, Wang L, Tang J (2021) Efficient removal of volatile organic compound by ball-milled biochars from different preparing conditions. J Hazard Mater 406:124676. https://doi.org/10.1016/j.jhazmat.2020.124676

Zouari M, Devallance DB, Marrot L (2022) effect of biochar addition on mechanical properties, thermal stability, and water resistance of hemp-polylactic acid (PLA) composites. Materials 15:2271–2287. https://doi.org/10.3390/ma15062271

Authors and Affiliations

M. Zouari[1,2] (ID) · **L. Marrot[1,3,4]** · **D. B. DeVallance[1,2,5]**

1   InnoRenew CoE, Livade 6a, 6310 Izola, Slovenia

2   Faculty of Mathematics Natural Sciences and Information Technologies, University of Primorska, Muzejski Trg 2, 6000 Koper, Slovenia

[3] University of Primorska, Andrej Marušic Institute, Muzejski Trg 2, 6000 Koper, Slovenia

[4] ZAG Fire Laboratory, Obrtna Cona Logatec 35, 1370 Logatec, Slovenia

[5] College of Science and Technology, Commonwealth University, 401 North Fairview Street, Lock Haven, PA 17745, USA